PAPER • **OPEN ACCESS**

Trapping Ba^+ with seven-fold enhanced efficiency utilizing an autoionizing resonance

To cite this article: Noah Greenberg *et al* 2024 *Quantum Sci. Technol.* **9** 035023

Quantum Science and Technology

PAPER

Trapping Ba^+ with seven-fold enhanced efficiency utilizing an autoionizing resonance

Noah Greenberg*, Brendan M White, Pei Jiang Low and Crystal Senko

Institute for Quantum Computing and Department of Physics & Astronomy, University of Waterloo, Waterloo, Ontario N2L 3G1, Canada

* Author to whom any correspondence should be addressed.

E-mail: noahgreenberg@me.com

Keywords: ion trap, barium, trapped ions, photoionization, autoionization, quantum information

OPEN ACCESS

RECEIVED
31 July 2023

REVISED
22 November 2023

ACCEPTED FOR PUBLICATION
16 April 2024

PUBLISHED
3 May 2024

Abstract

Trapped ions have emerged as a front runner in quantum information processing due to their identical nature, all-to-all connectivity, and high fidelity quantum operations. As current trapped ion technologies are scaled, it will be important to improve the efficiency of loading ions, especially when working with long chains of ions or rare isotopes. Here, we compare two different isotope-selective photoionization schemes for loading $^{138}Ba^+$ ions. We show that a two-step photoionization scheme ending in an autoionizing transition increases the ion loading rate nearly an order of magnitude compared to an established technique which does not excite an autoionizing state. Our novel photoionization scheme can be extended to all isotopes of barium. Given that autoionizing resonances exist in every trapped ion species, exploitation of this process is a promising pathway to increase the loading rates for trapped ion computers.

1. Introduction

Barium is a versatile quantum information carrier with the capacity to be used as an optical, metastable, or ground-state qubit [1]. Additionally, barium has been demonstrated as a *qudit*, controlling and reading out up to 13-levels [2] by taking advantage of its unusually long-lived metastable $5d\,^2D_{5/2}$ state [3]. The flexibility of the atomic structure in barium and the visible wavelengths used to drive the electric-dipole transitions are also attractive from a practical perspective [4]. All of these key features of barium, coupled with extraordinary experimental state-preparation and measurement results [5–8] have captured the attention of researchers and motivated the trapping of barium in the most sophisticated surface traps as a front-running platform for quantum information processing [9–12]. Unfortunately, a caveat of working with metallic barium is that it can oxidize within seconds when exposed to atmosphere, and specifically, the radioactive $^{133}Ba^+$ isotope can only be sourced as a salt and commonly used in microgram quantities. For these reasons, the focus of this work is on maximizing the loading rate of barium to quickly generate long chains of ions for quantum information processing utilizing laser ablation.

Typically, photoionization for trapping ions is done using resonance-enhanced multi-photon ionization [13]. This can involve a resonant 'first step', using a laser that drives an electronic transition in the neutral atom, along with a 'second step' using light that is sufficiently energetic to drive the electron from the excited state to the unbound continuum. We choose to use two different lasers for photoionization since it allows a small ionization volume to be defined, which reduces Doppler broadening and increases the isotope-selectivity. Isotope shifts in the first step transition are generally large enough (>10 MHz) so that only the target isotope of neutral atoms are excited and then ionized. Researchers have employed a variety of different first steps in two-step photoionization schemes for the isotope-selective loading of barium such as 413 nm and 554 nm [14], as well as 791 nm [15]. We opt to use 554 nm as our first step since it is a strong-dipole allowed transition and decays almost entirely back down to the $6s^2\,^1S_0$ state, which reduces the amount of dark atoms produced when repumping lasers are not present. We outline two relevant parameters for these first step transitions in table 1.

Table 1. Comparison of first steps used to drive a transition in neutral barium between the ground state, $6s^2\,{}^1S_0$, and an excited intermediate state, as part of a two-step photoionization process for loading Ba^+. The branching ratio represents the likelihood that an atom in the intermediate state will decay back to the ground state. In this work we use a 554 nm laser as the first step to drive a strong dipole-allowed transition, with a branching ratio almost entirely back down to the ground state.

λ (nm)	Intermediate state	Linewidth (MHz)	$6s^2\,{}^1S_0$ Branching ratio
413	$5d6p^3D_1$	9.15 ± 0.26 [16]	0.026(13) [16]
554	$6s6p^1P_1$	19.02 ± 0.19 [16]	0.9966(0.2) [16]
791	$6s6p^3P_1$	0.820 ± 0.050 [17]	0.38 [18]

Utilizing an autoionizing resonance for the second step can significantly enhance the photoionization cross-section. For this reason, autoionizing resonances are routinely exploited in Sr^+ experiments [19–21]. By contrast, previous work loading Ba^+ has typically used a non-resonant second step during the photoionization process (i.e. not ending in an autoionizing transition) [9, 22] or not utilized photoionization at all [23]. Non-resonant photoionization schemes ionize an electron directly into the continuum, while autoionizing schemes use a resonant transition to a quasi-bound state embedded in the continuum, which can provide up to an order of magnitude higher experimentally measured photoionization cross-sections [24]. This is advantageous considering the loading efficiency of an ion trap has been shown to be proportional to the photoionization cross-section [25]. Another plausible method to increase the loading rate of Ba^+ in trapped ion experiments is with the use of magneto-optical traps [26, 27], but this is more challenging due to the technical overhead and the large number of repumpers needed to create a closed cooling cycle in neutral barium [28].

Autoionizing resonances can be found in the ionization spectrum of all elements with two valence electrons, including barium. These resonances, which are found past the first ionization threshold, describe states where the wavefunctions of the electrons have become correlated [29, 30]. They are the result of interference between discrete states and the ionization continuum [31], and they are found as distinct peaks in the photoionization cross-section. Typically, the resonance is characterized as a Fano-profile [24], allowing useful information to be extracted from the measured cross-section. The energies and cross-sections of these resonances can be calculated with multi-channel quantum defect theory analysis [32–34] or an eigenchannel R-matrix method [35, 36]. The cross-sections have also been empirically measured [24, 37, 38].

If the photon energy $\hbar\omega$ of the second step is tuned to a known autoionizing resonance, then the two valence electrons will become doubly excited and enter a quasi-bound state Ba^{**} embedded in the ionization continuum with a lifetime, $\tau \ll 1$ ns:

$$\hbar\omega + \mathrm{Ba}\left(6s6p^1P_1\right) \rightarrow \mathrm{Ba}^{**} \rightarrow \mathrm{Ba}^+ + e^-. \tag{1}$$

In this manuscript, two different photoionization schemes are compared for isotope-selective loading of $^{138}Ba^+$ ions. Each scheme is a two-step process with the first step using 554 nm light to drive a strong dipole transition between the $6s^2\,{}^1S_0 \leftrightarrow 6s6p^1P_1$ states. The second step for ionization uses either a non-resonant photoionization scheme with 405 nm light, or an autoionizing scheme with light near 390 nm. We use 405 nm as the second step in the non-resonant scheme since it has been demonstrated by multiple groups due to the low cost of the laser [9, 22]. We use 390 nm as the second step in the autoionizing scheme since this, combined with 554 nm, has yielded the largest experimentally measured photoionization cross-section for barium [24]. There are many possible photoionization schemes that could be compared when trapping Ba^+. We choose to keep the first step of the photoionization scheme the same to more directly compare the impact on Ba^+ loading rates of varying the second step between a non-resonant transition and an autoionizing transition. The two schemes are presented in figure 1(a). We observe a seven-fold increase in the loading rate for $^{138}Ba^+$ ions when using the autoionizing scheme compared with the non-resonant scheme. Furthermore, the autoionizing scheme requires significantly lower intensity in the second step beam to trap chains of $^{138}Ba^+$, which reduces the likelihood of trap charging. The observed increase in loading rates is consistent with the increase in the previous experimentally measured photoionization cross-sections of the two compared photoionization schemes [24, 37, 38].

2. Experimental overview

The comparison of the two different photoionization schemes is conducted on a four-rod trap using IonControl software [39]. These experiments are performed using laser ablation on a naturally abundant, stable, salt ($BaCl_2$) target in an isotope-selective manner trapping $^{138}Ba^+$ [22]. Typically, $V_{DC} = 7 - 9$ V are applied to the needles, providing axial confinement of the ions. The voltage applied to the rods is $|V_{RF}| \approx 230$ V delivered at $\Omega_{RF} = 2\pi \times 20.772$ MHz by a helical resonator [40]. A pair of diagonal rods also

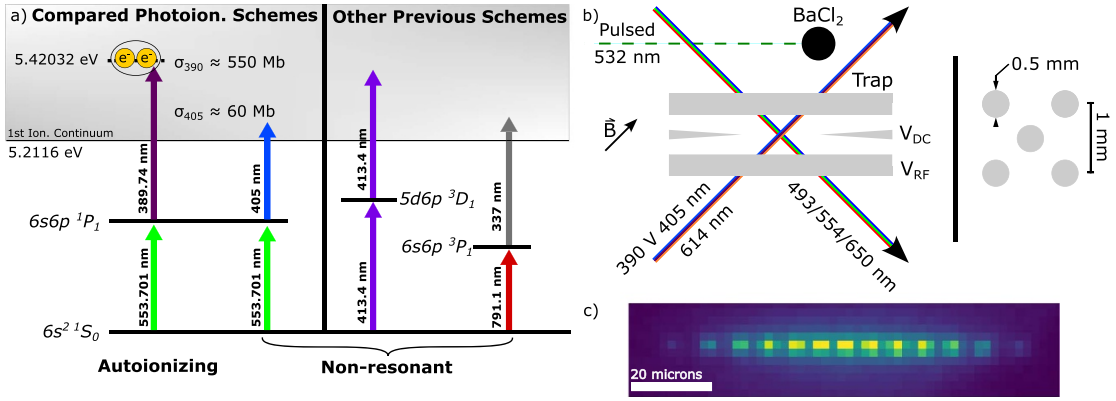

Figure 1. (a) Comparison of the two different photoionization schemes in the text, with the previously measured cross-sections σ_{390} and σ_{405} [24]. Each scheme uses the exact same first step, exciting neutral barium to the $6s6p^1P_1$ state. The second step varies depending on the scheme, either ending in an autoionizing resonance or somewhere in the continuum not resonant with a specific transition. The autoionizing state is represented by a line in the continuum. Other commonly used schemes for photoionizing barium are depicted for comparison. (b) Experimental overview of the trap and beam geometry. The trap needles are separated by 2.8 mm and the rods are spaced by 1 mm. The 554 nm beam is orthogonal to the atomic plume to reduce Doppler broadening and also orthogonal to the second ionization beam (either 390 or 405 nm) to reduce the ionization volume and thus trap charging. (c) A chain of thirteen $^{138}Ba^+$ ions trapped with a single ablation pulse using the autoionizing scheme. The outer ions sit far from the center of the beam, causing them to be dim compared to the center ions. Each pixel is $\approx 2\,\mu$m.

has an additional $V_{DC} = 3$ V applied. The secular radial frequencies for $\omega_{x,y}$ are $\approx 2\pi \times 1.2$ MHz and $2\pi \times 1.4$ MHz, respectively, and the axial frequency ω_z is $\approx 2\pi \times 100$ kHz.

There are three relevant beam paths, as depicted in figure 1(b). The first beam path is comprised of linearly polarized 493, 554, and 650 nm light focused to a beam waist of ~31, 35, 41 μm ($1/e^2$ radius), respectively. This path provides Doppler cooling via 493 nm using the $6s^2S_{1/2} \leftrightarrow 6p^2P_{1/2}$ transition, with 650 nm light used to repump $5d^2D_{3/2} \rightarrow 6p^2P_{1/2}$. The 554 nm laser is also in this path and it is used to drive the first step in the photoionization process. The typical laser powers are 110 ± 3, 15 ± 1, and $210 \pm 6\,\mu$W for the 493, 554, and 650 nm beams, respectively.

The second beam path consists of linearly polarized 390 or 405 nm light, as well as 614 nm light. This path intersects with the first beam path at the center of the trap. During any given experiment either 390 nm or 405 nm is used as the second photoionization step, but never both. In Ba^+, the $5d^2D_{5/2}$ state is populated within a few seconds of exposure to the 390 nm laser because the 390 nm beam is detuned by <1 nm from the $6p^2P_{1/2} \rightarrow 6d^2D_{3/2}$ transition. This can decay to $5d^2D_{5/2}$, so the 614 nm laser is used to repump $5d^2D_{5/2} \rightarrow 6p^2P_{3/2}$. The 614 nm beam carries $7 \pm 1\,\mu$W of power. It should be noted that the 614 nm laser is not necessary if the 390 nm beam is shuttered shortly after trapping. In this set of experiments, the 390 nm beam was not shuttered so the 614 nm laser was required for efficient cooling and ion detection. The beam waists were ~34 μm and ~35 μm for the 390 nm and 405 nm beams, respectively. The powers of the 390 nm and 405 nm beams vary depending on the experiment, but we only observe trapping above 150 μW in this setup using either laser.

As shown in figure 1(b), the third and final beam consists of only the 532 nm ablation laser. This is a nanosecond pulsed, flash-lamp pumped, Nd:YAG laser, capable of delivering up to 10 mJ of pulse energy, although we operate at much lower pulse energies, around 138 μJ. The beam waist of the ablation laser is 98 μm. Upon hitting the ablation target, this laser pulse causes sublimation of the $BaCl_2$, generating a vapor of atomic barium. The ablation target is oriented such that the surface norm is directed towards the trap center, which is 14.6 mm away [22]. The target contains $40 - 50$ mg worth of $BaCl_2$.

The 405 nm laser is a fiber-pigtailed Cobolt 06-MLD from HÜBNER Photonics GmbH. The 390 nm laser is a tunable Littrow laser from MOGLabs. Neither of the second step lasers were frequency locked. The frequencies of the first step for each isotope have already been measured in previous works [22]. The 554 nm light used to drive the first step transition is a frequency-doubled 1107 nm Cateye laser from MOGLabs. For trapping $^{138}Ba^+$, the 554 nm laser is locked to 541.433 04 THz. For most experiments, the 493 nm, 614 nm, and 650 nm lasers were locked to 607.425 99 THz, 487.989 67 THz, and 461.312 12 THz, respectively. Based on the frequency of the first step and previously measured photoionization cross-sections [41], where the autoionizing resonance occurs 5.420 32 eV above the $6s^2\,^1S_0$ state, the theoretical optimal target frequency for the 390 nm laser is calculated to be $\nu_{390} = 769.193\,88$ THz. The resonance is >50 GHz wide, which exceeds the mode-hop free tuning range of the 390 nm Littrow laser, so no attempt was made to rigorously quantify the loading rate as a function of frequency. In practice, the 390 nm laser was simply tuned to

$\nu_{390} \pm 19$ GHz, and a significant increase in the loading rate of $^{138}Ba^+$ was observed, which is detailed in the following sections.

For ablation loading of the ion trap, the following experimental procedure is employed:

(i) The RF and DC trap voltages are turned on and the laser frequencies are set for $^{138}Ba^+$. The trap potential and DC voltages are kept on when trapping.
(ii) The ablation laser sends a single pulse to the target. Approximately, $10 - 15\,\mu$s later, the majority of the atomic flux reaches the trapping region where the atoms either pass through or are photoionized by the two-step process.
(iii) Doppler cooling sweeps are implemented in order to cool and crystallize hot ions that may have been trapped. This is done by red-detuning the 493 nm cooling beam $100 - 500$ MHz and sweeping within five seconds back to the previously stated lock point. This corresponds to a detuning of $5 - 25 \times \gamma_{493}$, the natural linewidth transition.
(iv) Steps (ii)–(iii) are repeated until an ion is trapped.

Fluorescent light from neutral atoms and ions is collected by a 0.26 NA home-built objective and sent to either a photo-multiplier tube (H10682-210) or a charge-coupled device (BFLY-PGE-05S2M-CS). Typically, experiments were run with light being sent to the photo-multiplier tube to quickly determine whether an ion had been trapped. To count how many ions were trapped, the collected light is sent to the charge-coupled device to image the ion chain, as shown in figure 1(c).

3. Results

3.1. Loading saturation & fluence experiments

The following section compares the loading rates of the two photoionization schemes as the second step power is varied, thus changing the intensity experienced by the neutral atoms. We find that the loading rate saturates in the autoionizing scheme at lower intensities compared to the non-resonant scheme. Similarly, we vary the ablation laser power and find that the autoionizing scheme can load ions with significantly lower ablation fluence. Typically, we work with intensities on the second-step photoionization beam up to $\sim 75\,\mathrm{W\,cm^{-2}}$. In this regime, if the second-step frequency is not resonant with an autoionizing transition, the photoionization cross-section is so small that the loading rate scales linearly with second-step laser intensity.

The loading rates of $^{138}Ba^+$ (ions/pulse) as a function of intensity for both photoionization schemes are depicted in figure 2(a). Below $10\,\mathrm{W\,cm^{-2}}$ the autoionizing and non-resonant photoionization schemes converge to a loading rate of zero. But at higher intensity, the loading rate saturates when utilizing the autoionizing transition and significantly outperforms that of the non-resonant scheme. Saturation of the loading rate using the autoionizing transition occurs at $\sim 63.7\,\mathrm{W\,cm^{-2}}$ with a loading rate of roughly 5 ions/pulse. Based on a linear fit, the non-resonant scheme would require an intensity of $\sim 630\,\mathrm{W\,cm^{-2}}$ to achieve a similar loading rate.

The loading saturation intensity parameter I_{sat} can be calculated using the fitted Fano linewidth parameter $\Gamma \approx 60.4 \pm 1$ GHz [24],

$$I_{\mathrm{sat}} = \frac{\hbar\omega^3\Gamma}{4\pi c^2} \approx 63.7\,\mathrm{W\,cm^{-2}} \tag{2}$$

where c is the speed of light and $\omega = 2\pi \cdot 769.193$ THz is the measured angular frequency of the light. Our results agree well with the calculated saturation parameter, as shown in figure 2(a). The ablation laser pulse fluence was kept constant throughout the loading saturation experiments at $0.45 \pm 0.01\,\mathrm{J\,cm^{-2}}$.

Figure 2(b) shows the loading rate of $^{138}Ba^+$ as a function of ablation laser fluence. The ablation laser fluence experiments were conducted with $\sim 53 \pm 3\,\mathrm{W\,cm^{-2}}$ and $\sim 66 \pm 2\,\mathrm{W\,cm^{-2}}$ average intensity for the 405 nm and 390 nm beams, respectively. As the laser fluence increases so does the amount of neutral atoms and ions produced. If the fluence is too low, loading can be difficult, but if it is too high, ions can be trapped directly [22]. There are three main regions considered when conducting the ablation loading experiments. Region I ($<0.3\,\mathrm{J\,cm^{-2}}$) is a region of low laser fluence in which there is minimal loading of $^{138}Ba^+$ ions. We were not able to load in this region using the non-resonant scheme after 100 attempts; however, we were able to successfully load after 53 attempts using the autoionizing scheme. Region II ($0.3 - 0.45\,\mathrm{J\,cm^{-2}}$) is the ideal operating fluence for trapping, since it produces enough neutral atom flux to trap in an isotope-selective manner, but not enough ablation-produced ions to load directly. Region III ($>0.45\,\mathrm{J\,cm^{-2}}$) is a region of high fluence which produces a significant amount of ions from the ablation process itself, drastically reducing isotope-selectivity since ions can be loaded directly into the trap. These regions are not hard limits, but act mostly as guidelines for these experiments.

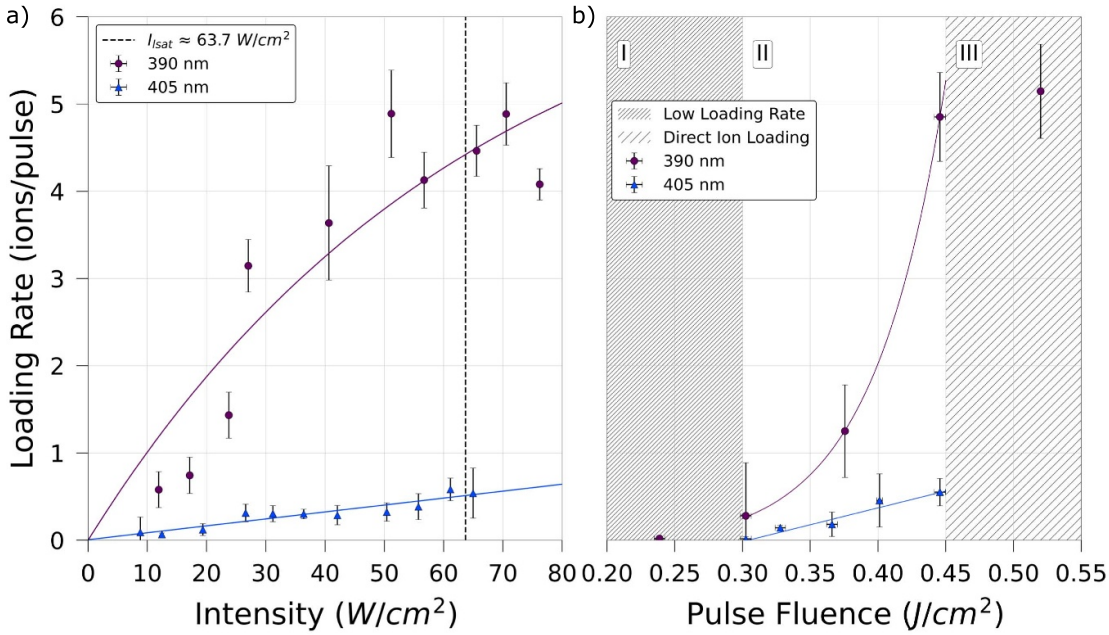

Figure 2. (a) Loading rates of $^{138}Ba^+$ as a function of intensity in the second step laser. The calculated I_{sat} of the autoionizing transition is denoted by the dashed line. The fit to the autoionizing transition assumes the loading rate follows an exponential of the type $f(x) = a(1 - e^{-b \cdot x})$, where $a \approx 7.097$ ions/pulse and $b \approx 0.015\,cm^2W^{-1}$ are fitted constants and x is intensity in $W\,cm^{-2}$ [37]. The fit predicts $f(1/b) \approx 4.5$, which agrees well with the calculated loading saturation parameter $f(I_{sat}) \approx 4.4$. The fit to the non-resonant 405 nm loading rate is linear. The error bars represent the standard error of the mean. The ablation fluence was $\sim 0.45\,J\,cm^{-2}$. The 390 nm laser frequency was tuned to $769.193\,88 \pm 0.019$ THz. (b) Loading rates of $^{138}Ba^+$ as a function of ablation fluence. We operate primarily in Region II. The regions are described further in the text. The intensity of the second step photoionization beam is $\sim 53.5\,W\,cm^{-2}$ for these measurements. The lines act simply as visual guides. The 390 nm laser frequency was measured to be $769.209\,05 \pm 0.000\,40$ THz.

3.2. Optimized loading rates

In this section, we compare the loading rates of $^{138}Ba^+$ with ideal and similar laser parameters. For these experiments, the ablation fluence was set to $0.45\,J\,cm^{-2}$ and the average intensities of the second step 405 and 390 nm photoionizing beams were $I_{405} \approx 56 \pm 7\,W\,cm^{-2}$ and $I_{390} \approx 65 \pm 12\,W\,cm^{-2}$. The intensities used in the experiments were chosen such that the loading rate using the 390 nm laser would be saturated.

The likelihood of trapping long chains of $^{138}Ba^+$ was greatly increased using the autoionizing scheme, which is evident by the increase in the average ions per pulse. Roughly one out of five attempts succeeded in trapping using the non-resonant scheme, while nine out of ten attempts succeeded using the autoionizing scheme. The average loading rates with the standard deviation are $R_{405} = 0.43 \pm 0.81$ ions/pulse and $R_{390} = 4.48 \pm 2.75$ ions/pulse using the non-resonant and autoionizing schemes, respectively. These rates are compared in figure 3. The median ions trapped per pulse is 0 ions for the non-resonant scheme and 4 ions for the autoionizing scheme.

The loading rates quoted above cannot be directly compared to infer the enhancement from the autoionizing resonance, because the intensities of the second-step lasers and the quantity of neutral atoms produced during ablation were not identical across both sets of experiments. During the loading experiments, we monitor the rate of fluorescence at 554 nm after each ablation laser pulse, as a proxy for the flux of neutral barium atoms. We observed higher neutral atom flux for the experiments conducted with the autoionizing scheme than with the non-resonant scheme (up to 39.5% higher fluorescence counts at 554 nm), which we attribute to natural variations in the number of ablated atoms. We make the simplifying assumption that the probability of trapping is proportional to both the neutral atom flux and the average second-step intensity, when the ionization rate is far from saturation [22]. Thus, we estimate that the loading rate using 405 nm would have been $R'_{405} \approx 0.66$ ions/pulse, if the neutral atom flux and second-step laser power had been identical to those in the 390 nm experiments. We therefore calculate that the increase in loading rate of $^{138}Ba^+$ using the autoionizing scheme is a factor of $R_{390}/R'_{405} \approx 6.8$. This compares well with the ratio of photoionization cross-sections, which have previously been measured as $\sigma_{390}/\sigma_{405} = 520\,Mb/75\,Mb \approx 6.9$ [24] and $550\,Mb/60\,Mb \approx 9.2$ [38].

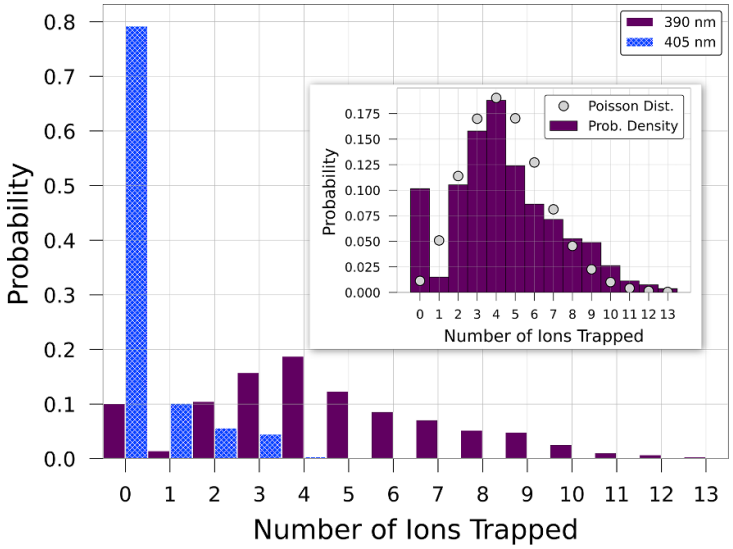

Figure 3. Histogram of the loading rates of $^{138}Ba^{+}$, where each event is a single ablation pulse and trapping attempt. The average loading rate using the autoionizing scheme is $R_{390} = 4.48 \pm 2.75$ ions/pulse and the average loading rate using the non-resonant scheme is $R_{405} = 0.43 \pm 0.81$ ions/pulse. There are 265 and 266 trapping attempts for the non-resonant and autoionizing scheme, respectively. The inset shows the probability of loading using the autoionizing scheme fitted to a Poisson distribution. The 390 nm laser frequency was tuned to 769.193 88 ± 0.018 THz.

4. Discussion

The demonstrated autoionizing scheme using 554 and 390 nm lasers retains the isotope-selectivity previously presented in [22], since it utilizes the same first step, which is the isotope-selective step in the photoionization process. We conducted a brief study to confirm this, where 478 ions (minimum of two $^{138}Ba^{+}$ ions in the chain, a total of 114 unique ion chains) were analyzed for dark or dim ions, which indicate the presence of other ion isotopes besides $^{138}Ba^{+}$. We found that only 8 ions in all of these chains were other isotopes. This puts a maximum bound on the isotope-selectivity for $^{138}Ba^{+}$ of 98%, which is consistent with previous studies [22]. To achieve high loading rates, the first transition in the ionization sequence is usually power broadened significantly, which limits isotope selectivity [22]. Thus, using this more efficient autoionizing scheme and lowering the power of the first step laser may allow for better isotope selectivity with similar loading rates in the future.

We briefly investigated the loading rates of the $^{137}Ba^{+}$ isotope with the autoionizing scheme. A significant increase in the loading rate, with a factor of at least 5, was immediately apparent for the autoionizing scheme. However, we did not make a controlled quantitative comparison between the two schemes for this isotope. This photoionization scheme can also be applied to $^{133}Ba^{+}$ since the autoionizing transition is broad enough that it makes any isotope shifts between $^{138}Ba^{+}$, $^{137}Ba^{+}$, and $^{133}Ba^{+}$ negligible.

The linewidth of the measured autoionizing resonance is ∼60 GHz, but we found a considerable increase in the loading rate even when the frequency of the 390 nm laser was >100 GHz detuned from the ideal frequency for driving the transition calculated to be at 769.193 88 THz. So in practice, tuning anywhere near this resonance can result in a significant increase in the loading rate. In fact, the autoionizing transition is so broad that precision control of the laser frequency and linewidth are not required. However, under optimal conditions, exploiting autoionizing resonances can ionize atoms with ionization efficiencies near 100% [42].

There are many autoionizing resonances embedded in the first ionization continuum of barium that can be used for efficient photoionization. Assuming 554 nm is the first step in a two-step photoionization scheme, the best second step is to utilize the strongest autoionizing resonance, as this will most efficiently ionize the neutral atoms and allow for lower intensities to be used. Other possible autoionizing states that are easily accessible from the intermediate $6s6p^1P_1$ state are outlined in table 2.

There are other first steps that can be used besides 554 nm to drive to an intermediate state before exciting an autoionizing state embedded in the continuum. This includes, but is not limited to, the $5d6p^3D_1$ state driven with 413 nm light [43] and the $6s6p^3P_1$ state driven with 791 nm light [38]. The strongest resonance in the photoionization cross-section utilizing the $6s6p^3P_1$ intermediate state has been measured to be 102 ± 15 Mb using 340 nm as the second step [38]. This is a significantly strong resonance, but its cross-section is still considerably lower than the 550 Mb cross-section using $6s6p^1P_1$ as the intermediate state with 390 nm, which is demonstrated in this manuscript. There are also considerable resonances in the

Table 2. Comparison of some previously measured autoionizing resonances when using $6s6p^1P_1$ as the intermediate state. Other intermediate states can be used, but the strongest experimentally measured photoionization cross-section of barium utilizes $6s6p^1P_1$ as the intermediate state. The energy is relative to the $6s^2\,^1S_0$ ground state.

Wavelength (nm)	Cross-section (Mb)	Autoion. State [41]	Energy (eV) [24]
380.75	≈ 300 [24]	$5d_{3/2}9d\,(J=0)$	5.49 549
384.33	≈ 290 [24]	$5d_{3/2}9d\,(J=1)$	5.46 516
389.74	550 [24], 520 ± 78 [38]	$5d_{5/2}8d(J=1)$	5.42 032
402.92	370 [24], 300 ± 45 [38]	$5d_{3/2}8d(J=1)$	5.31 629

photoionization spectrum of barium using $5d6p^3D_1$ as an intermediate state, for which relative cross-sections have been measured [43].

5. Conclusion

We have demonstrated an efficient isotope-selective photoionization scheme for trapping barium ions utilizing an autoionizing resonance, motivated by the $^{137}Ba^+$ and elusive $^{133}Ba^+$ isotopes. The increase in loading rates (ions/pulse) compared with previous ablation studies are consistent with previously measured photoionization cross-sections of barium and equate to a seven-fold enhancement in the loading rate of $^{138}Ba^+$ ions. This photoionization scheme will aid in the consistent trapping of long chains of barium ions and will help enable NISQ era devices to be built based on rare isotopes like $^{133}Ba^+$. Furthermore, the demonstrated advantage of using autoionizing resonances allows researchers to efficiently ionize neutral atoms at significantly lower intensities, reducing the risk of trap charging.

Data availability statement

The data that support the findings of this study are openly available at the following URL/DOI: 10.5281/zenodo.11051404.

Acknowledgments

This research was supported in part by the Natural Sciences and Engineering Research Council of Canada (NSERC) and the Canada First Research Excellence Fund (CFREF). We would like to thank Dr Jens Lassen for his initial suggestion and for pointing out the existence of these autoionizing resonances as well as ongoing discussion related to the experiment. We thank Dr Akbar Jahangiri Jozani, Nicholas Zutt, and Xinghe Tan for reviewing the manuscript.

Conflict of interest

The authors declare no conflicts of interest.

ORCID iDs

Noah Greenberg https://orcid.org/0000-0001-9912-8159
Brendan M White https://orcid.org/0000-0003-4605-8235

References

[1] Allcock D T C, Campbell W C, Chiaverini J, Chuang I L, Hudson E R, Moore I D, Ransford A, Roman C, Sage J M and Wineland D J 2021 Omg blueprint for trapped ion quantum computing with metastable states *Appl. Phys. Lett.* **119** 214002
[2] Jiang Low P, White B and Senko C 2023 Control and readout of a 13-level trapped ion qudit (arXiv:2306.03340)
[3] Madej A A and Sankey J D 1990 Quantum jumps and the single trapped barium ion: determination of collisional quenching rates for the $5d^2\,D_{5/2}$ level *Phys. Rev.* A **41** 2621–30
[4] Binai-Motlagh A, Day M, Videnov N, Greenberg N, Senko C and Islam R 2023 A guided light system for agile individual addressing of Ba^+ qubits with 10^{-4} level intensity crosstalk *Quantum. Sci. Technol.* **8** 4
[5] Hucul D, Christensen J E, Hudson E R and Campbell W C 2017 Spectroscopy of a synthetic trapped ion qubit *Phys. Rev. Lett.* **119** 100501
[6] Christensen J E, Hucul D, Campbell W C and Hudson E R 2020 High-fidelity manipulation of a qubit enabled by a manufactured nucleus *npj Quantum Inf.* **6** 35
[7] Christensen J E 2020 High-fidelity operation of a radioactive trapped ion qubit, ^{133}Ba *PhD Thesis* University of California
[8] An F A, Ransford A, Schaffer A, Sletten L R, Gaebler J, Hostetter J and Vittorini G 2022 High fidelity state preparation and measurement of ion hyperfine qubits with $i > \frac{1}{2}$ *Phys. Rev. Lett.* **129** 130501

[9] Shi X, Todaro S L, Mintzer G L, Bruzewicz C D, Chiaverini J and Chuang I L 2023 Ablation loading of barium ions into a surface electrode trap *Appl. Phys. Lett.* **122** 264002
[10] Leibrandt D R, Clark R J, Labaziewicz J, Antohi P, Bakr W, Brown K R and Chuang I L 2007 Laser ablation loading of a surface-electrode ion trap *Phys. Rev.* A **76** 055403
[11] Graham R D, Chen S-P, Sakrejda T, Wright J, Zhou Z and Blinov B B 2014 A system for trapping barium ions in a microfabricated surface trap *AIP Adv.* **4** 057124
[12] Hendricks R J, Grant D M, Herskind P F, Dantan A and Drewsen M 2007 An all-optical ion-loading technique for scalable microtrap architectures *Appl. Phys.* B **88** 507–13
[13] Ashfold M N R and Western C M 1999 Multiphoton spectroscopy, applications *Encyclopedia of Spectroscopy and Spectrometry* ed J C Lindon (Elsevier) pp 1424–33
[14] Leschhorn G, Hasegawa T and Schaetz T 2012 Efficient photo-ionization for barium ion trapping using a dipole-allowed resonant two-photon transition *Appl. Phys.* B **108** 159–65
[15] Wang B, Zhang J W, Gao C and Wang L J 2011 Highly efficient and isotope selective photo-ionization of barium atoms using diode laser and LED light *Opt. Express* **19** 16438
[16] Niggli S and Huber M C 1987 Transition probabilities in neutral barium *Phys. Rev.* A **35** 2908–18
[17] Akulshin A M, Celikov A A and Velichansky V L 1992 Nonlinear Doppler-free spectroscopy of the 6^1S_0-6^3P_1 intercombination transition in barium *Opt. Commun.* **93** 54–58
[18] Dzuba V A, Flambaum V V and Ginges J S M 2000 Calculation of parity and time invariance violation in the radium atom *Phys. Rev.* A **61** 062509
[19] Putterman S and Kirilov E 2009 Two-photon ionization for efficient seeding and trapping of strontium ions *Eur. Phys. J.* D **54** 683–91
[20] Vant K, Chiaverini J, Lybarger W and Berkeland D J 2006 Photoionization of strontium for trapped-ion quantum information processing (arXiv:quant-ph/0607055)
[21] Osada A and Noguchi A 2022 Deterministic loading of a single strontium ion into a surface electrode trap using pulsed laser ablation *J. Phys. Commun.* **6** 015007
[22] White B M, Jiang Low P, de Sereville Y, Day M L, Greenberg N, Rademacher R and Senko C 2022 Isotope-selective laser ablation ion-trap loading of $^{137}Ba^+$ using a $BaCl_2$ target *Phys. Rev.* A **105** 033102
[23] Olmschenk S and Becker P 2017 Laser ablation production of Ba, Ca, Dy, Er, La, Lu and Yb ions *Appl. Phys.* B **123** 1–6
[24] Willke B and Kock M 1993 Measurement of photoionization cross sections from the laser-excited Ba I (6s6p) $^1P_1^0$ state *J. Phys. B: At. Mol. Opt. Phys.* **26** 1129
[25] Deslauriers L *et al* 2006 Efficient photoionization loading of trapped ions with ultrafast pulses *Phys. Rev.* A **74** 063421
[26] Cetina M, Grier A, Campbell J, Chuang I and Vuletić V 2007 Bright source of cold ions for surface-electrode traps *Phys. Rev.* A **76** 041401
[27] Moses S A *et al* 2023 A race track trapped-ion quantum processor *Phys. Rev. X.* **13** 041052
[28] De S, Dammalapati U, Jungmann K and Willmann L 2009 Magneto-optical trapping of barium *Phys. Rev.* A **79** 041402
[29] Shenstone A G 1931 Ultra-ionization potentials in mercury vapor *Phys. Rev.* **38** 873–5
[30] Fano U 1983 Correlations of two excited electrons *Rep. Prog. Phys.* **46** 97
[31] Fano U 1961 Effects of configuration interaction on intensities and phase shifts *Phys. Rev.* **124** 1866–78
[32] Aymar M 1990 Eigenchannel R-matrix calculation of the J = 1 odd-parity spectrum of barium *J. Phys. B: At. Mol. Opt. Phys.* **23** 2697
[33] Aymar M and Robaux O 1979 Multichannel quantum-defect analysis of the bound even-parity J = 2 spectrum of neutral barium *J. Phys. B: At. Mol. Phys.* **12** 531
[34] Aymar M, Greene C H and Luc-Koenig E 1996 Multichannel Rydberg spectroscopy of complex atoms *Rev. Mod. Phys.* **68** 1015–123
[35] Greene C H and Theodosiou C E 1990 Photoionization of the Ba 6s6p $^1P_1$ state *Phys. Rev.* A **42** 5773–5
[36] Greene C H and Aymar M 1991 Spin-orbit effects in the heavy alkaline-earth atoms *Phys. Rev.* A **44** 1773–90
[37] He L-W, Burkhardt C E, Ciocca M, Leventhal J J and Manson S T 1991 Absolute cross sections for the photoionization of the 6s6p ^1P excited state of barium *Phys. Rev. Lett.* **67** 2131–4
[38] Ali Kalyar M M 2008 Two-step Laser Excitation Studies of Bound and Autoionizing States in Barium *PhD Thesis* Quaid-i-Azam University
[39] Maunz P, Mizrahi J and Goldberg J 2016 Ioncontrol v. 1.0, version 00
[40] Low P J 2019 Tolerable experimental imperfections for a quadrupole blade ion trap and practical qudit gates with trapped ions *Master's Thesis* University of Waterloo
[41] Camus P, Dieulin M, El Himdy A and Aymar M 1983 Two-step optogalvanic spectroscopy of neutral barium: observation and interpretation of the even levels above the 6*s* ionization limit between 5.2 and 7 eV *Phys. Scr.* **27** 125
[42] Payne M G and Hurst G S 1985 *Theory of Resonance Ionization Spectroscopy* (Springer) pp 183–8
[43] Armstrong D J, Wood R P and Greene C H 1993 Photoionization of the $5d6p\,^3D_1$ state of barium *Phys. Rev.* A **47** 1981–8